International Journal of Greenhouse Gas Control 114 (2022) 103589

Contents lists available at ScienceDirect

International Journal of Greenhouse Gas Control

journal homepage: www.elsevier.com/locate/ijggc

Towards defining reasonable minimum composition thresholds – Impacts of variable CO_2 stream compositions on transport, injection and storage

Heike Rütters [a], Sebastian Fischer [b,*], Le Quynh Hoa [c], Dirk Bettge [c], Ralph Bäßler [c], Jobst Maßmann [a], Christian Ostertag-Henning [a], J. Lennard Wolf [a], Martin Pumpa [d], Udo Lubenau [d], Sandra Knauer [e], Philip Jaeger [e], Andreas Neumann [f], Kristoff Svensson [f], Herbert Pöllmann [f], Christof Lempp [f], Flora F. Menezes [f], Birger Hagemann [g]

[a] Federal Institute for Geosciences and Natural Resources (BGR), Stilleweg 2, D-30655, Hannover, Germany
[b] Federal Institute for Geosciences and Natural Resources (BGR), Wilhelmstr. 25-30, D-13593, Berlin, Germany
[c] Federal Institute for Materials Research and Testing (BAM), Unter den Eichen 87, D-12205, Berlin, Germany
[d] DBI Gas- und Umwelttechnik GmbH, Karl-Heine-Str. 109/111, D-04229, Leipzig, Germany
[e] Eurotechnica GmbH, An den Stücken 55, D-22941, Bargteheide, Germany
[f] Institute of Geosciences and Geography, Martin-Luther University Halle-Wittenberg, Von-Seckendorff-Platz 3, D-06120, Halle/Saale, Germany
[g] Institute of Subsurface Energy Systems (ITE), Clausthal University of Technology, Agricolastraße 10, D-38678, Clausthal-Zellerfeld, Germany

ARTICLE INFO

Keywords:
Impurities
CO_2 quality
Pipeline network
Whole-chain CCS scenario
Recommendations

ABSTRACT

To set up recommendations on how to define "reasonable minimum composition thresholds" for CO_2 streams to access CO_2 pipeline networks, we investigated potential impacts of CO_2 streams with different and temporally variable compositions and mass flow rates along the CCS chain. All investigations were based on a generic "CCS cluster scenario" in which CO_2 streams captured from a spatial cluster of eleven emitters (seven fossil-fired power plants, two cement plants, one refinery and one steel mill) are collected in a regional pipeline network. The resulting CO_2 stream (19.78 Mio t impure CO_2 per year) is transported in a trunk line (onshore and offshore) and injected into five generic replicate storage structures (Buntsandstein saline aquifers) offshore. Experimental investigations and modeling of selected impacts revealed beneficial as well as adverse impacts of different impurities and their combinations. Overall, no fundamental technical obstacles for transporting, injecting and storing CO_2 streams of the considered variable compositions and mass flow rates were observed. We recommend to define minimum composition thresholds for each specific CCS project through limiting i) the overall CO_2 content, ii) maximum contents of relevant impurities or elements, iii) acceptable variability of concentrations of critical impurities, and defining impurity combinations to be avoided.

1. Introduction

The composition of CO_2 streams captured at large stationary emitters depends on the emitter, the capture technology and further purification, conditioning and compression steps applied prior to transport. Presence of impurities will modify thermophysical and transport properties as well as chemical behavior of CO_2 streams with implications on CO_2 transport (e.g., Munkjord et al., 2016; Peletiri et al., 2017), injection and storage (e.g., Talman et al., 2015; ISO/TR27921:2020). In the last decade, impacts of individual impurities or binary/ternary impurity mixtures on CO_2 transport and storage were studied in detail by experimental and modeling work to optimize capture and purification efforts and costs without compromising transport and storage safety (e.g., Brunsvold et al., 2016; Porter et al., 2016; Rütters et al., 2016). When CO_2 streams from different emitters are fed into a large-scale transport and storage infrastructure, the costs of CO_2 transport and storage may be lowered significantly (e.g. ZEP, 2011; IEA GHG, 2015). Hence, the economic benefit for a CCS project will increase with i) higher impurity levels that are acceptable for transport and storage and ii) higher numbers of emitters sharing one common transport and storage infrastructure. To share a common CO_2 transport and storage infrastructure, CO_2 streams can be collected from a regional cluster of CO_2 emitters, as is envisaged, for example, in the PORTHOS CCUS project (NL; e.g., Neele et al., 2018), the Net Zero Teesside project (UK; e.g., Hunter,

* Corresponding author.
E-mail address: sebastian.fischer@bgr.de (S. Fischer).

https://doi.org/10.1016/j.ijggc.2022.103589
Received 12 May 2021; Received in revised form 24 November 2021; Accepted 19 January 2022
Available online 1 February 2022

2021) and the Alberta Carbon Trunk Line (CA; e.g. Wheler et al., 2020). Alternatively, a transport and storage hub may be established with individual CO_2 transport (by ship or pipeline) from each emitter to the hub as planned in the Norwegian Northern Lights project (NO; e.g., Gassnova, 2020). Feeding CO_2 streams of different composition and with variable mass flow rates into a joint transport and storage infrastructure results in a temporal variation of both CO_2 stream composition and mass flow rate in that infrastructure (e.g., Kahlke et al., 2020; Spitz et al., 2018). These temporal variations may cause additional downstream impacts in comparison to streams of constant composition and mass flow rates that have to be considered for the specification of acceptable CO_2 stream qualities for larger transport and storage infrastructures.

In this line, the collaborative project CLUSTER focused on investigating selected impacts of CO_2 streams with temporally variable mass flow rates and compositions on CO_2 transport, injection and storage based on dedicated laboratory experiments and innovative model simulations. The basis of these investigations was a regional CCS cluster scenario (see Section 2). The overall aim of the CLUSTER project was to set up recommendations on how to define "reasonable minimum composition thresholds" that CO_2 streams should meet when accessing CO_2 transport pipelines or pipeline networks (according to EU Directive 2009/31/EC).

In this paper, selected results of the CLUSTER project and the derived recommendations are presented. All results of the CLUSTER project can be found in more detail in Rütters et al. (2019) and references therein.

2. CCS cluster scenario

As a basis for the experimental and modeling work in the CLUSTER project, a CCS cluster scenario was defined. The scenario was set up based on actual regional givens in Germany (Rütters et al., 2019).

The CCS cluster scenario includes a generic regional cluster of eleven CO_2 emitters (Fig. 1). The regional cluster comprises CO_2 emitters from energy sector as well as industry: power plants using hard coal (two plants), lignite (three plants) and natural gas (two plants), an integrated iron and steel plant, two cement plants and one refinery. Individual CO_2 emitters have been equipped with different capture technologies (post-combustion, pre-combustion and oxyfuel; Kather et al., 2019). In total, 19.78 Mio t CO_2 (including impurities) are captured in the emitter cluster annually. The captured CO_2 streams are transported in a regional pipeline network that consists of several feed lines ("collection network", cf. Fig. 1). Individual pipe segments in the collection network have lengths between 4 km and 22 km adding up to a total length of 160 km. An onshore trunk line with a length of 300 km composed of three sections, each equipped with a pumping station at the beginning, connects the regional cluster with the coastline. Off the coast, a 100 km long offshore pipeline on the sea floor (temperature: 278 K) transports the CO_2 to the injection site. At the point of injection, a generic CO_2 storage reservoir within the Buntsandstein is assumed (see below).

For each CO_2 emitter, CO_2 stream compositions as well as temporally varying mass flow rates were defined (see also Kather et al., 2019; Rütters et al., 2019). Due to the emitters' operating profiles, CO_2 stream compositions (and mass flow rates) vary in the subsequent transport and storage infrastructure (see also Kahlke et al., 2020). For example, throughout the year, the CO_2 concentration in the stream were modelled to fluctuate between 98.72 and 99.93% mol around a mean value of 99.29% mol in the transport network; modelled trunk line mass flow rates varied between 1033 and 3236 t/h with an annual average of 2252 t/h (see also Rütters et al., 2019).

Based on modelled maximum and minimum concentrations of each impurity in the pipeline network and the trunk line, two CO_2 stream compositions were determined and used for subsequent studies within the CLUSTER project. These comprise minimum and maximum concentrations of impurities with oxidizing and reducing properties – termed "reducing" mixture and "oxidizing" mixture, respectively (Table 1). Following results of Rütters et al. (2016), the H_2O content was limited to ≤ 50 ppm_v in all fed-in CO_2 streams to prevent acid formation and limit pipeline corrosion (see also Section 3.2).

As a basis for investigations of selected impacts of variable CO_2 stream compositions and mass flow rates on CO_2 injection and storage, a generalized geological model was set up. This geological model includes a generic lithological succession of stratigraphic units that are based on real data from the German North Sea region. For injection and storage, an anticlinal structure within the Buntsandstein was chosen. Two sandstone units within this structure at a depth of 1.600 m below surface were defined as storage reservoir. For reservoir sandstone and the other stratigraphic units, mineralogical compositions as well as values for porosities and permeabilities were assigned based on literature data (details are given in Rütters et al., 2019). For the storage reservoir, a temperature of 333 K and a pressure of 16 MPa were assumed. Based on the defined parameters, a storage capacity of approximately 250 Mio t (pure) CO_2 was estimated for the storage reservoir. Thus, five analogous storage structures are needed to accommodate the entire amount of CO_2 captured annually in the CCS cluster scenario over the foreseen injection period of 30 years. For laboratory experiments, so-called Grauer Wesersandstein (GWS; Trendelburger Sandstein, Mittlerer Buntsandstein; Weber and Ricken, 2005) was used as sample material. This sandstone is mainly composed of quartz, various feldspars, and muscovite with minor amounts of, e.g., apatite, beidellite, illite, and chlorite. Effective porosities were mostly between 10.6 and 13.1% with gas permeabilities ranging from 1.3 to 21.5 mD. In some model simulations as well as in storage capacity estimations, an "averaged" sandstone composition of Buntsandstein from the North German Basin (Waldmann et al., 2014) with higher porosities (up to 28.7%) and permeabilities (up to approx. 700 mD) was used.

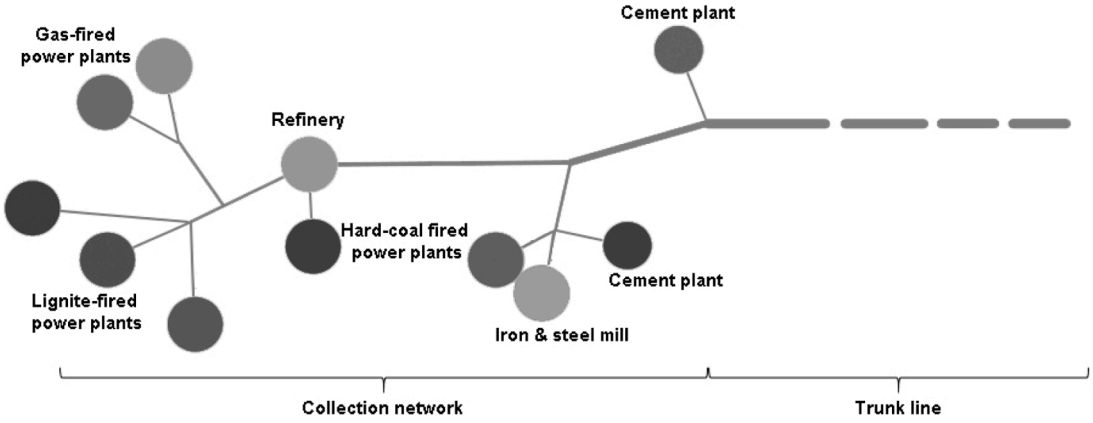

Fig. 1. Schematic sketch of plant locations and the transport network as defined in the CCS cluster scenario (not to scale; modified after Lubenau et al., 2019).

Table 1
Impurity concentration ranges for impact studies on CO_2 transport, injection and storage derived from modelled minimum and maximum concentrations in different parts of the project's CCS cluster scenario (see also Rütters et al., 2019).

	Transport			Injection/Storage		
Mixture characteristic	Reducing	Oxidizing	Simplified	Reducing	Oxidizing	Simplified
CO_2	98.55	98.56	ad 100	98.94	98.94	ad 100
N_2	0.3700	0.5300	–	0.4460	0.4760	–
O_2	–	0.6700	0 - 0.670	–	0.3030	0 - 0.3030
Ar	0.0260	0.2200	–	0.2600	0.2650	–
NO_2	–	0.0100	0 - 0.010	–	0.0055	0 - 0.0055
SO_2	–	0.0070	0 - 0.007	–	0.0030	0 - 0.0030
CO	0.0400	0.0030	–	0.0150	0.0028	–
H_2	1.0000	–	0 - 1.00	0.3330	–	0 - 0.3330
CH_4	–	–	–	–	–	–
H_2S	0.0050	–	–	0.0017	–	–
COS	–	–	–	–	–	–
H_2O	0.0050	0.0050	0.0050	0.0050	0.0050	0.0050

3. Impacts on CO_2 pipeline transport

3.1. Transport network dimensioning & designing

The pipeline transport system was simulated with an in house developed MATLAB tool (see also Lubenau et al., 2019; tool not publically available). In brief, the tool identifies the design parameters of pipeline segments and intermediate pumps based on the mass flow rates to be transported and a maximum allowed flow velocity of 3 m/s (cf. API, 1991). Further, a minimum pressure is required throughout the pipeline transport system to prevent unwanted phase transition during transport (e.g., Peletiri et al., 2018). The thermodynamic properties of the impure CO_2 streams are calculated with an external library (REFPROP; Lemmon et al., 2013) employing the GERG 2008 equation of state (Kunz and Wagner, 2012).

The pressure in the pipeline transport system varies i) over time due to variations in the mass flow rates and ii) over the length of the transportation path due to friction with the inner pipeline surface: At a ground temperature of 288 K, calculated pressures vary between 5.5 and 12.5 MPa at the collection network exit and entry, respectively. Based on the calculated pressure distribution, the quantities of CO_2 to be transported and the calculated fluid properties of the impure CO_2 streams, the tool selects pipeline dimensions from a list of predefined standard dimensions for the chosen carbon steel L485MB (X70) according to DIN EN 10208–2:2009. Whereas the calculated inner diameters of the trunk line are nearly the same for the transport of pure and impure CO_2 in our scenario, differences in calculated wall thicknesses were more pronounced since required pipeline entry pressures were lower in case of pure CO_2, so that in this case a thinner pipeline wall can be chosen (Fig. 2).

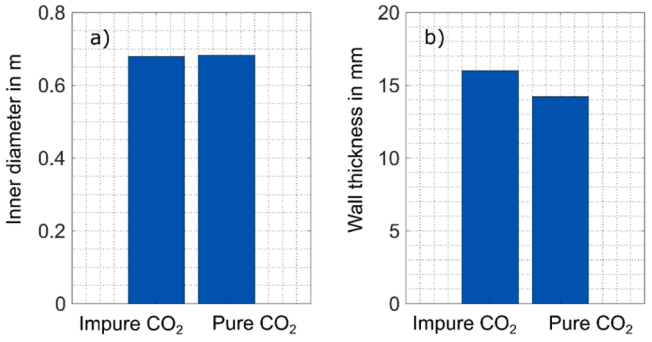

Fig. 2. Dimensioning of the trunk line's 100 km segments (a) inner diameter; b) wall thickness) for the transport of the entire amount of impure CO_2 captured in the CCS cluster scenario taking into account maximum calculated mass flow rates and variations in CO_2 stream compositions. For comparison, dimensions for the transport of the same amount of pure CO_2 are given.

3.2. Chemical reactions within CO_2 streams

The co-occurrence of different impurities in CO_2 streams may lead to chemical reactions in the stream during pipeline transport (e.g. Peletiri et al., 2019; Morland et al., 2019a). Due to the comparatively short residence times, i.e. few 100 hours, of the impure CO_2 stream within the pipeline in our scenario, a computational approach based on thermodynamic equilibria is not suitable for the prediction of chemical reactions in CO_2 streams. This holds especially true for the formation of inorganic acids that may trigger corrosion processes. For instance, the local co-occurrence of H_2 and O_2 would thermodynamically result in their stoichiometric conversion to H_2O. Hence, a kinetic approach was used in this study to estimate reaction yields. For this, common first and second order rate laws with input data taken from literature (see below) were used to create a set of ordinary differential equations (ODE) to predict the concentration-time profiles of each impurity and the reaction products. The ODEs were solved by a one-step Euler solution algorithm written in MATLAB® ("chemical simulation algorithm"; not publically available). Computations were performed for "closed CO_2 cells" with different compositions and residence times in the pipeline at a temperature of 288 K. Diffusive or convective mixing as well as laminar flow velocities were not taken into account. The data for the kinetic rate laws were mostly taken from studies on atmospheric reactions (e.g., Atkinson et al., 2004) or combustion processes (e.g., Baulch et al., 1992). Accordingly, oxidative reactions are rather well represented in our kinetic modeling, while data of reductive reactions especially including H_2 are rather scarce. Literature data for the kinetic rate laws had to be adapted or extrapolated to the considered (partial) pressure, redox and temperature conditions of pipeline transport. For simplification, the simulations include only reactions within the CO_2 stream; i.e. formation of condensed phases (on pipeline surfaces) was not considered. Implementation of the "chemical simulation algorithm" in the MATLAB tool for simulation of the pipeline transport system (see Section 3.1) allowed estimating CO_2 stream compositions in different parts of the pipeline system (Fig. 3).

Given the assumptions and simplifications used for these chemical model simulations, the processes identified as relevant and the overall tendencies in concentration changes should be considered rather than specific numbers. In this line, the overall results of these numerical simulations can be summarized as follows: The key impurity for acid formation is H_2O. On the timescale of seconds to minutes, any H_2O in the CO_2 stream is predicted to be consumed forming inorganic acids such as H_2SO_4 or HNO_3, if SO_x and/or NO_x are available. This acid formation involves cross-chemical reactions between various redox-active impurities. Only SO_3 will be directly and rapidly converted to H_2SO_4. The slow oxidation of SO_2 to SO_3 by O_2 or the direct oxidation of H_2SO_3 to H_2SO_4 were found not to be competitive on the timescale of pipeline transport. Therefore, the initial ratios of SO_x (and of SO_3:SO_x), NO_x and

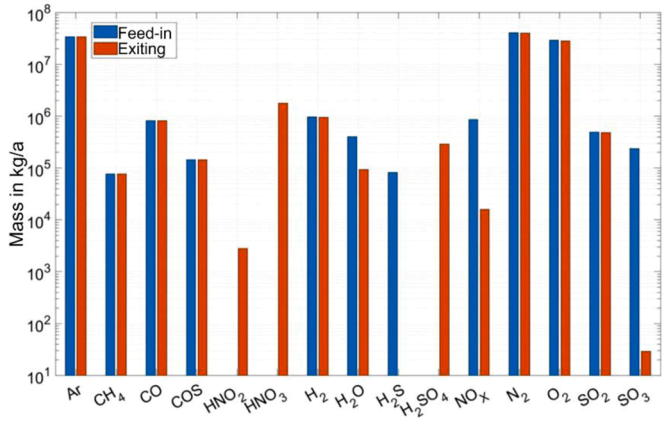

Fig. 3. Simulated cumulative amounts of impurities exiting the trunk line in one year in comparison to impurity amounts fed into pipeline network by all emitters per year.

H_2O mainly control the total amount and the component distribution of formed acids. Thus, acid formation can be limited if, for example, the CO_2 stream is kept near-dry. These simulation results are in line with recent experimental data of, e.g., Morland et al. (2019b): In their experiments CO_2-impurity mixtures of SO_2, O_2, H_2S and H_2O were found to be stable at 10 MPa and 25 °C, only the presence of both H_2S and NO_2 in the mixtures triggered cross-chemical reactions. When all assessed impurities were present together in concentrations of 35 ppm_v or higher, a formation and condensation of strong acids was observed that potentially cause corrosion of carbon steel (Morland et al., 2019b).

3.3. Reactive and non-reactive wetting of metallic materials

If any formed fluid droplet in the pipeline will remain and spread on the inner pipeline surface or will be mobilized and transported further with the CO_2 stream is depending on, amongst other things, the wetting behavior of the fluid. In case of corrosive fluids, the longer the residence time of a droplet, the more likely the occurrence of corrosion processes. The wetting behavior of a system that consists of a low density fluid ("vapor") phase (v), a higher-density fluid (liquid, l) and a solid (s) phase is controlled by the interaction between these three phases. It can be described by the contact angle θ between the tangent of the liquid-vapor interphase A_{lv} and the one of the liquid-solid-interphase A_{sl} at the three phase contact point (see Fig. 4).

The contact angles of distilled H_2O drops on a carbon steel (X70) or a martensitic steel (S41500) in a pure CO_2 atmosphere were analyzed with the sessile drop method (for a more detailed description of the procedure, see also Knauer et al., 2019) as a function of pressure and time at a temperature of 278 K. The measurements were performed at thermal equilibrium. For both steels, the contact angle increases with increasing pressure (see Fig. 5). At low to moderate pressures, the increase of contact angles is steep starting at a value of ~70 ° and reaching ~120 ° at 5 MPa. At pressures above 5 MPa, the contact angle only increases by ~10 ° in the range up to 20 MPa. This principally different behavior is due to differences in the CO_2 fluid states: Apparently, a partly-wetting system ($\theta < 90$ °) occurs in presence of low-density (gaseous) CO_2,

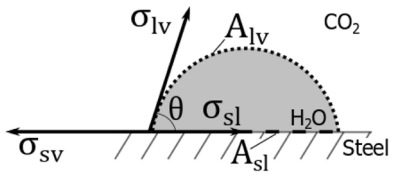

Fig. 4. Schematic representation of a H_2O drop onto a steel surface in a CO_2 atmosphere.

and a non-wetting system ($\theta > 90$ °) in dense-phase (liquid) CO_2. The different fluid states of CO_2 mostly affect the energies σ_{lv} and σ_{sv} between the vapor phase (i.e. CO_2 phase) and the liquid (i.e. H_2O drop) as well as the solid phase (i.e. steel), respectively. Both energies decrease with increasing pressure. Considering the Young equation (Young, 1805), diminishing σ_{lv} as well as σ_{sv} leads to higher contact angles. The measurements were performed with the first drop being dispensed and placed onto the steel sample, giving no time for any chemical reactions. The influence of time was determined in a separate series of experiments in which the drop was left on the steel surface for at least 10 minutes. A decrease in contact angle by ~20 ° was observed over this time on both steels under investigation, independent of pressure. After 10 minutes only negligible additional changes in contact angle were observed. In the experiment with the pipeline steel X70, the drop of CO_2-saturated H_2O reacted with the metal surface forming $FeCO_3$ (see also Le et al., 2018). The corrosion layer affects surface heterogeneity and roughness and thus the contact angle. No corrosion occurs on the alloy S41500, so that the surface remains unchanged, but the surface energies are modified due to adsorptive effects, leading to a shift of the three-phase contact line and a decrease of the contact angle. The results show that the carbon steel X70 is subject to a reactive wetting behavior, because the wetting is influenced by reactions between the solid substrate and the drop liquid, i.e. by the formation of a corrosion layer (cf. Kumar and Prabhu, 2007). In contrast, the martensitic steel S41500 displays a non-reactive behavior. Due to the observed complex interplay between wetting and corrosion, this should be studied in detail at the relevant conditions during the selection of pipeline steels.

At least three different drops were analyzed individually to determine the contact angle. The measurements were performed with non-water saturated CO_2 phases to mimic the transient processes of real systems. Due to diffusion of water into the CO_2 phase, the drop volume decreased during the experiment. However, the observed volume decrease was negligibly small, so that this effect is not discussed any further here.

3.4. Corrosion of metallic materials

Despite its low corrosion resistance, carbon steel has been widely used for process piping due to its low cost, availability, machinability and good mechanical properties (e.g., Ratnayaka et al., 2009; Stewart, 2016). Previous studies have shown that CO_2 transport pipelines manufactured of carbon steels are highly at risk when exposed to CO_2 streams containing corrosive impurities such as O_2, SO_x, NO_x, H_2 and H_2S in combination with H_2O concentrations higher than 600 ppm_v (e.g. Rütters et al., 2016). Exposure tests were performed within the project CLUSTER using impurity-containing CO_2 streams at temperatures of 288 K and 278 K (resembling those in the onshore and offshore parts of the trunk line, respectively). At these low temperatures, even low concentrations of H_2O can lead to acid formation and condensation, mainly of sulfuric/sulfurous and nitric acids Eq. (1)–(5), due to localized temperature variation and cross-reactions between H_2O and impurities (Choi et al., 2010; ISO/TR27921:2020; Hua et al., 2018; Kratzig et al., 2020; Morland et al., 2019a, b, c):

$$SO_2 + H_2O \rightleftharpoons H_2SO_3 \quad (1)$$

$$SO_2 + NO_2 \rightarrow SO_3 + NO \quad (2)$$

$$2\,NO + O_2 \rightarrow 2\,NO_2 \quad (3)$$

$$SO_3 + H_2O \rightarrow H_2SO_4 \quad (4)$$

$$3\,NO_2 + H_2O \rightarrow 2\,HNO_3 + NO \quad (5)$$

For the tests, coupons were machined from the as-received pipeline sections, mechanically ground using 60, 120, and then 320 grit silicon carbide abrasive papers, cleaned with ethanol, degreased with acetone

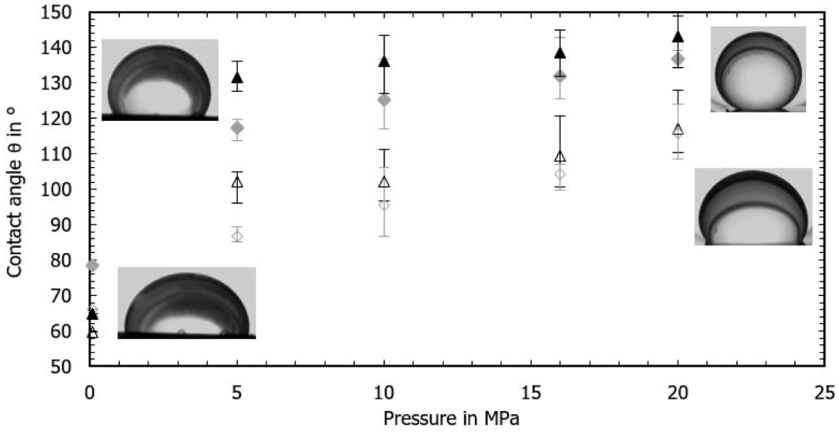

Fig. 5. Measured contact angles θ over pressure on carbon steel X70 (◆) and martensitic steel S41500 (▲) (averages from triplicate measurements; modified after Knauer et al., 2019). Filled symbols display measurements at t = 0 min and hollow symbols at t = 10 min. The individual images show an H_2O drop on the alloy S41500 surface at a pressure of 5 MPa and temperature of 278 K at t = 0 min (top left) and t = 10 min (bottom left), respectively, and at a pressure of 20 MPa and temperature of 278 K at t = 0 min (top right) and t = 10 min (bottom right), respectively.

and dried up with N_2 prior to every test. Corroded coupons were taken out from autoclave and immediately stored in a desiccator under vacuum until analysis. During exposure to the test mixtures (simplified oxidizing mixture (Table 1): 50 ppm_v H_2O, 70 ppm_v SO_2, 6700 ppm_v O_2, 100 ppm_v NO_2, as well as a simplified reducing mixture (cf. Table 1): 50 ppm_v H_2O, 1% H_2 and 50 ppm_v H_2S, and a mixture of both), L485MB/X70 coupons taken from a real pipeline piece showed mainly uniform and partially localized corrosion with rates of less than 0.1 mm a^{-1} after 1000 h at a pressure of 10 MPa and a temperature of 278 K. The corrosion rates decrease in the order oxidative + reductive (0.055 mm a^{-1}) > oxidative (0.045 mm a^{-1}) >> reductive (0.006 mm a^{-1}) mixture, indicating not only the importance of cross-reactions for corrosion processes, but also the major role of oxidative impurities (see also Kratzig et al., 2018). Different from high temperature tests, the

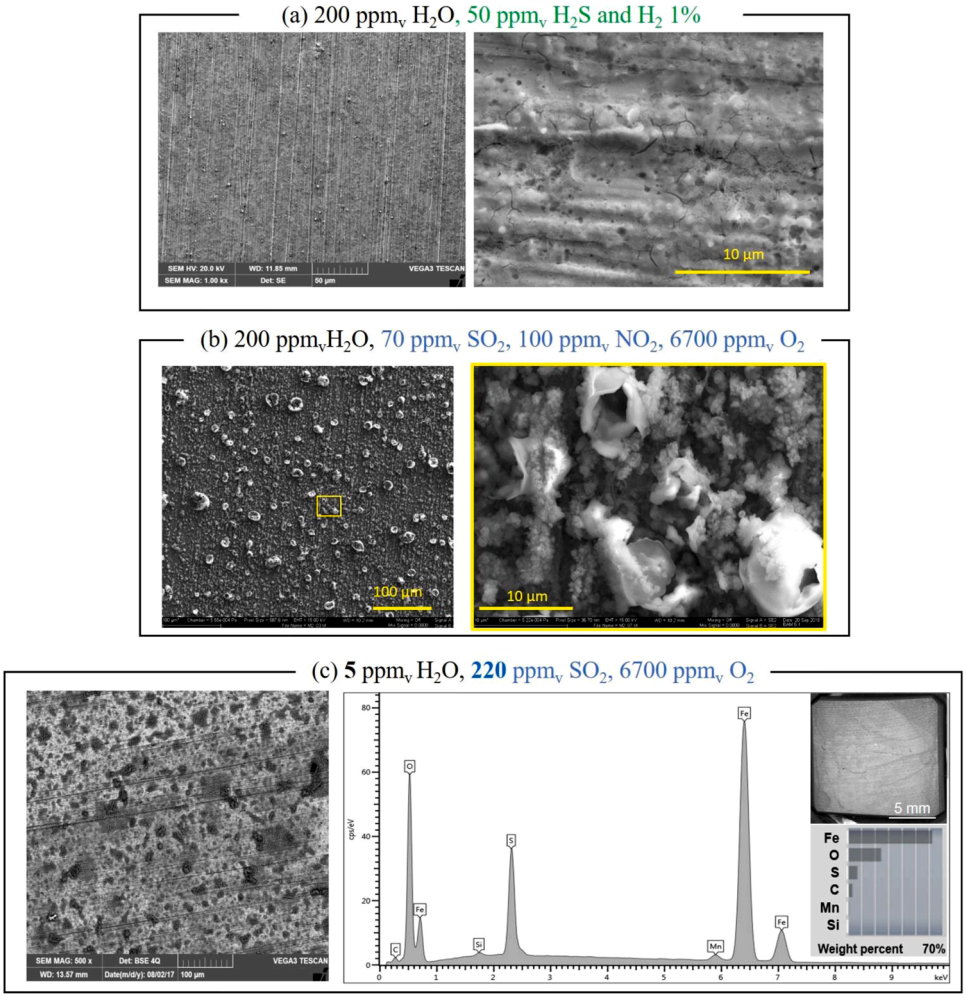

Fig. 6. Scanning electron microscope (SEM, VEGA3 TESCAN, Czech Republic) images of L485MB coupons taken from a real pipeline piece exposed for seven days in different dense-phase CO_2-impurity mixtures (compositions as specified in figure parts a, b and c) at a pressure of 10 MPa and a temperature of 278 K. For mixture c, also EDS analysis results of corrosion products are presented.

corrosion products formed at 278 K are X-ray amorphous, powdery, and loosely attached and therefore provide no protection to the steel. It is noteworthy to mention that corrosion was observed to start at grinding line/surface defects and then progressed to larger areas. At the same temperature, pressure and flow rate, progression depended on the supply of impurities and the roughness of metal surface (see also Le et al., 2018). Since the wetting behavior depends strongly on the situation at the steel surface, initial corrosion products, although only small spots, can make surfaces much more reactive to wetting, promoting condensation processes later on (see also Knauer et al., 2019; Le et al., 2018). During transport in pipeline networks, mixing of CO_2 streams from different emitters may happen, leading to a small local increase of H_2O concentration as a result of cross reactions, e.g. $2\ H_2S + SO_2 \rightarrow 3\ S + 2\ H_2O$. An increase of the H_2O concentration from 50 to 200 ppm_v in the experiments resulted in a significant covering of the metal surface by corrosion products consisting mainly of iron sulfides (Fig. 6a) and hydrated iron nitrates, sulfates and oxyhydroxide/oxides (Fig. 6b) after 7 days of exposure. When H_2O concentrations were kept as low as 5 ppm_v (and in absence of NO_2), a SO_2 concentration of 220 ppm_v (three times the maximum CCS cluster scenario value) resulted only in spot-like corrosion products consisting of hydrated iron sulfate as revealed by Energy Dispersive X-Ray analysis (EDS, Aztec software, Oxford Instruments) (Fig. 6c). These results illustrate the importance of controlling concentrations of H_2O and reactive impurities along the transport pipeline network as also pointed out, for example, in the technical report ISO/TR27921:2020 and references therein.

3.5. Techno-economic considerations

The MATLAB tool described in Section 3.1 determines the design parameters for pipelines and pumps in the considered transport network. With this information, the same tool also calculates the costs of CO_2 transport, comprising capital and operational costs of the pipelines and pumps in the CCS system as well as the operational costs for the initial compression of the CO_2 stream to pressures between 6.69 and 13.09 MPa depending on the emitter's position in the network. A detailed investigation of different parameters potentially affecting transport costs showed, for example, a cost optimum (i.e. minimum specific transport costs) at a maximum tolerable flow velocity of 2 m/s for the considered transport scenario taking into account the range of surface roughnesses that may be encountered during the assumed pipeline operation time of 20 years (Fig. 7). At flow velocities > 3 m/s, that exceed the recommended maximum flow velocity for pipeline transport (API, 1991), a pronounced increase of specific transport costs was calculated. The surface roughness itself only marginally influenced specific transport costs.

In our analysis, lower inlet pressures were determined in the pipeline sections for pure CO_2 than for impure CO_2 streams. This made it possible to use pipes with thinner walls (see also Section 3.1). However, reducing the wall thickness had a negligible influence on the overall transport costs that are dominated in our transport scenario by the operational costs for initial compression and intermediate pumping. By investigating different CO_2 feed-in scenarios, it became apparent that the degree of capacity utilization of the pipeline system over the year plays a much greater role for the total transport costs than the purity of the CO_2 stream (see also Lubenau et al., 2019).

4. Impacts on CO_2 injection

4.1. Injection scenarios and mechanical implications

In order to analyze i) the migration of the injected CO_2 in the storage reservoir and ii) its physical impacts on the development of the pressure field as well as iii) the integrity of the cap rock, a new mathematical model for hydraulic-mechanically coupled processes, considering two-phase-flow, was developed (see also Grunwald et al., 2020) and implemented in the open source code OpenGeoSys (Kolditz et al., 2012). A generic geological model, derived from realistic stratigraphic and selected petrophysical properties of the German North Sea (Kaufmann et al., 2014; Wolf et al., 2015), was used as the basis for assessing several injection scenarios. A 2D vertical axisymmetric model was set up with a thickness of 32.3 m and a horizontal extent of 10 km representing the storage horizon in an anticlinal structure. In this simplified model, the cap rock is assumed impermeable and only the storage formation is discretized. Although the outer boundaries of the model are hydraulically open assuming constant gas and capillary pressures, the injected CO_2 is predicted to remain within the anticline within the simulated time period of 300 years (for details, see also Fuhrmann et al., 2019).

Three injection scenarios are exemplarily described in this paper: a constant injection rate is assumed in scenario A, which could represent a pipeline transport with some temporary buffer storage option; a variable injection rate is used in scenario B, based on the CCS cluster scenario (see above). CO_2 transport by ship could lead to a cyclically fluctuating injection, which characterizes scenario C. The amount of CO_2 injected per year is the same in all scenarios (mean injection rate: 125 $kg/s = 450$ t/h).

The pressure development in the storage reservoir shows a significant and rapid increase in all scenarios: Within the first injection day,

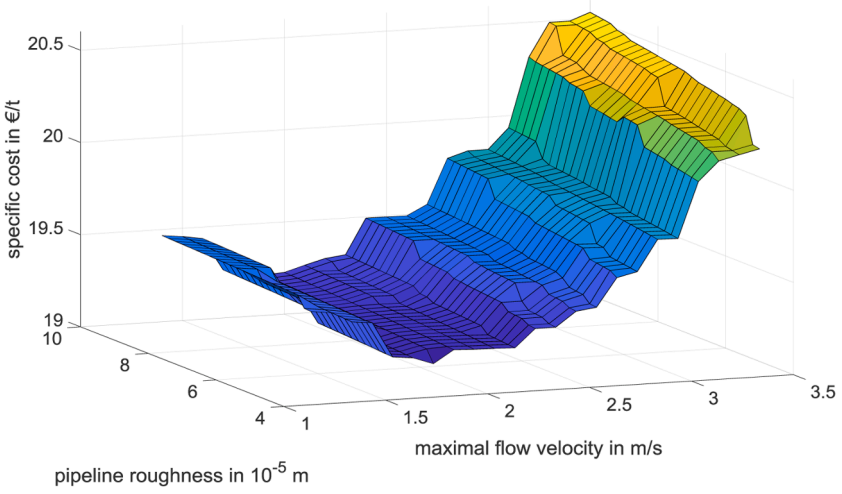

Fig. 7. Dependency of total specific transportation cost per t CO_2 (as the sum of capital and operational costs) on roughness of the inner pipeline surface and maximum allowed flow velocity in the considered transport scenario. Note the different zoom-factors of the axes.

the pressure at the top of the storage reservoir close to the injection well builds up to about 80% of its maximum value that is reached after approx. 500 days of injection. As an indicator for the mechanical stress on the cap rock due to CO_2 injection, a safety factor (SF) was defined as the ratio between the minimal principal stress in the rock and the pore pressure. If SF is lower than 1.0, the pore pressure is higher than the compressive stress in the rock and consequently tensile failure could occur. Fig. 8 shows the SF development over time, evaluated in the cap rock. Due to the temporarily high injection rates, the integrity of the cap rock is impaired around day 20 and 50 in scenario B.

The results of this numerical study are based on representative, generic material parameters; the resulting pore pressures are especially sensitive to the considered relations between capillary pressure and gas saturation as well as permeability and gas saturation. The model simulations indicate that CO_2 can be safely injected and stored in the defined generic storage reservoir, if fluctuations of CO_2 mass flow rates are within the range considered in the CCS cluster scenario. To store the entire amount of CO_2 collected in the emitter cluster, five replicates of this generic storage reservoir are needed (cf. Section 2).

4.2. Injectivity – laboratory experiments

The influence of possible geochemical reactions on the hydraulic properties of storage rocks in the vicinity of the CO_2 injection well was investigated by performing two-phase flow experiments with different CO_2 stream compositions at a pressure 16 MPa and a temperature of 333 K. In the flow cell, selected rock core samples (diameter: 3 cm; length: 6 and 24 cm) of the Grauer Wesersandstein were saturated with a synthetic brine (total salt content of 250 kg/m^3, NaCl: 230 kg/m^3, $CaCl_2$: 15 kg/m^3, $MgCl_2$: 5 kg/m^3). Subsequently, CO_2 with different combinations of impurities (0.003 mol% SO_2 and/or 0.3 mol% O_2) was injected with a constant rate of 0.5 ml/h over up to two weeks. Differential pressures across the rock cores were observed, which reflect the two-phase displacement process at the beginning of the experiment. A capillary threshold pressure of around 0.03 MPa had to be applied to force the CO_2 phase to enter the brine-saturated rock samples. The initial displacement process took around three hours. After the breakthrough of the CO_2 phase, the differential pressure decreased slowly until it stabilized at around 0.02 MPa. This value was reached after two and three days, respectively. An assessment of the hydraulic properties of the rock samples, i.e. porosity and permeability, was done before and after the experiments. The detailed description of the experimental setup, procedure and measured results can be found in Hagemann et al. (2018). With exception of one experiment, the changes in porosity and permeability before and after the experiments are very small and probably within the measurement precision. No trend of a potential permeability increase or decrease was identified. However, the porosity slightly increased in all experiments. One reason for this behavior could be the crumbling of unconsolidated grains during sample handling, which may adulterate the porosity measurement. Salt precipitation was the only geochemical effect identified during the flow experiments. During the flushing of the rock cores with distilled H_2O after the experiments, it was noted that a very high differential pressure builds up initially. This differential pressure was approximately twice as large as during the saturation process before the experiments and then rapidly reduced to the same value as after initial saturation. The salt precipitation potentially occurred during the experiments when the residual brine dried out because the H_2O dissolved in the CO_2 phase. However, no significant differences in the differential pressure during benchmark experiments with distilled H_2O were observed indicating that the main flow pathways for the CO_2 phase remain open. In conclusion, the investigated reservoir rock would be applicable for the storage of CO_2 with impurities (SO_2 and O_2) in the considered concentrations. No losses of injectivity due to geochemical alteration of the minerals near injection wells may be expected for this kind of rock material. These findings are in line with those of Pearce et al. (2016 & 2019) who also found minor impacts of impurities in CO_2 on siliciclastic reservoir rocks.

4.3. Corrosive processes at the cement-steel interface

To ensure the durability of completions and cement plugs of CO_2 injection wells, materials need to be compatible with formation waters (i.e. brine) and wells have to be constructed thoroughly to avoid excessive cement alteration and casing corrosion. It is well-known that CO_2 (with oxidative and acidic impurities such as SO_2, NO_2) and brine can change cement properties (e.g., Bachu and Bennion, 2009). There are two options to ensure cement durability: (1) use of a highly acid-resistant cement or (2) use of a cement that cures with CO_2 (see also Section 4.4). To test the first option, Dyckerhoff Variodur® cement was chosen in this study instead of common Portland cement to produce a highly acid-resistant mortar. For option 2, wollastonite (>96.5 wt.% $CaSiO_3$) was investigated, since this type of cement can react with CO_2 in the presence of an aqueous fluid to form $CaCO_3$ and silica (see also Svensson et al., 2019a). To study the corrosion of the steel-cement interface, representative low-cost pipeline materials including carbon steel L485MB/X70 (1.8977) and low alloyed steel 42CrMo4 (1.7225) were embedded in the investigated mortars to mimic a realistic steel casing-cement interface. For each steel type, eight samples were prepared (curing time: > 28 days). The samples were exposed to CO_2-saturated synthetic formation water at a pressure of 10 MPa and a temperature of 333 K for up to 140 days. Unfortunately, using only wollastonite proved not to produce a good binding to steel, thus an optimization of extra binding materials was needed in this cement system. In contrast to wollastonite, the mortar made of Variodur and

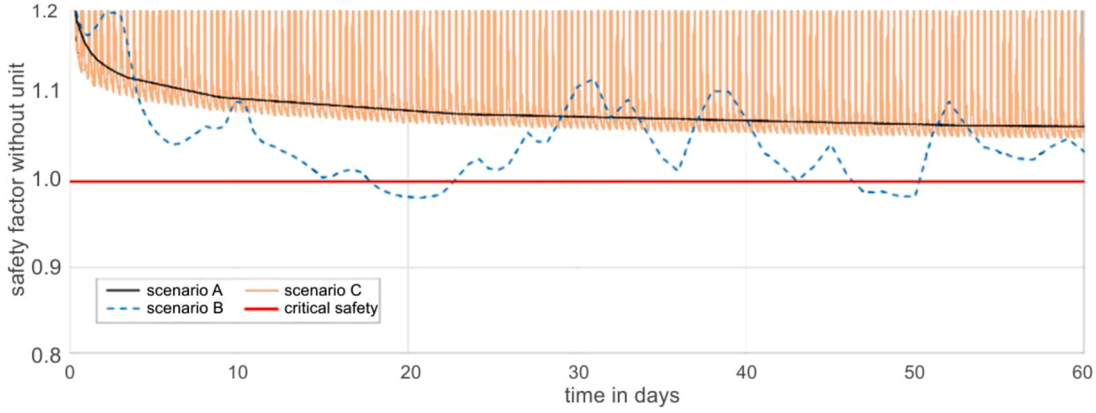

Fig. 8. Temporal development of the dimensionless safety factor (SF) within the first 60 days of injection. SF below 1.0 (red line) indicates a possible occurrence of tensile failure within the cap rock. Different injection scenarios are considered: constant (A), varying (B) and cyclically fluctuating (C) injection rate.

standard sand showed a dense and firm binding to the steel surface. Microscopic cross-sections of the mortar-steel interface revealed the porous structure of the mortar, indicating a possibility of CO_2 diffusion and intrusion of synthetic formation water between steel and mortar. Although the steel surface is passivated when in contact with the mortar due to the high pH value (~13) of the cement pore water, corrosion can occur at the exposed metal surface at the contact point between steel, mortar and brine (triple point) and progress along the interface (Figs. 9 & 10), somewhat similar to crevice corrosion (Kelly and Lee, 2018). This happened earlier than direct pitting due to the intrusion of chloride through the capillary pores of the mortar.

Despite its better pitting resistance performance in comparison to L485MB (see also Le et al., 2021), the low-alloyed 42CrMo4 still suffered from crevice corrosion when exposed to CO_2-saturated brine as can be seen from element mapping of the mortar-steel interface (Fig. 10). Mapped element concentrations clearly show an increased dissolution of Fe and Cr from the steel into the brine-bearing mortar from 10 weeks (Fig. 10a) to 20 weeks (Fig. 10b) of exposure, and vice versa an intrusion of chloride from the brine into the steel. This indicates the need of using high-alloyed steels in those well parts that are in direct contact with formation water and CO_2.

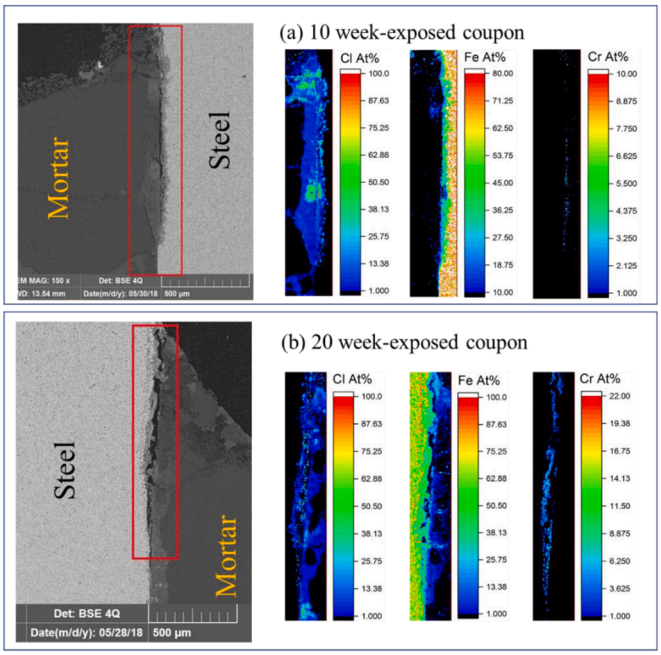

Fig. 10. EDS element mapping at the mortar-steel interface of the (a) 10 and (b) 20-week exposed 42CrMo4/Variodur coupons (embedded in fluorescencing epoxy resin, cut and ground, cleaned and dried up before imaging). The areas in the red boxes in backscattered electron images (left) were mapped and are presented on the right side.

4.4. Interaction of impure CO_2 with cementitious materials

Compressive strengths of standard mortar prisms prepared with a CEM III/A 52,5 N HS/NA (slag) cement (resistant against acids, low alkali content) were tested according to DIN EN 196–1:2005. For five weeks, the standard mortar prisms were put in an autoclave system filled with impure CO_2 and chloride-rich brine at a temperature of 333 K and a pressure of 16 MPa. After exposure, the compressive strengths were analyzed again. Additionally, SEM (Scanning Electron Microscopy) analysis was performed to detect changes of the mortar microstructure. In an innovative approach, wollastonite powder was either mixed with H_2O or brine and carbonated in an autoclave (at 333 K, CO_2 pressure of 2 MPa, 3 to 24 h, cf. Fig. 11a). The composition of the resulting material was analyzed by PXRD (Powder X-ray diffraction) and DSC/TG (Differential Scanning Calorimetry/Thermogravimetry) before and after the treatment. An in-depth description of test conditions and applied analytics is given in Svensson et al. (2018, 2019a, 2019b, 2020).

The treated CEM III prisms showed no loss of compressive strength (Fig. 11b) disregarding the composition of the formation water (brine: NaCl: 230 mg/l, $CaCl_2$: 15 mg/l, $MgCl_2$: 5 mg/l; weak brine: NaCl: 23 mg/l, $CaCl_2$: 15 mg/l, $MgCl_2$: 5 mg/l). Despite this finding, in all treated samples a formation of hydrocalumite ($[Ca_8Al_4(OH)_{24}][(Cl)(CO_3)(OH)] \cdot 8\ H_2O$) was observed in the pores in addition to the usual cement hydration products (Fig. 12). Hydrocalumite formed due to the reaction of the mortar with CO_2 and brine (see also Svensson et al., 2020).

In the other approach testing wollastonite curing with CO_2 in aqueous solution (see also Section 4.3), the wollastonite content decreased with time, while the carbonate content increased. The investigated CO_2 phase and brine compositions had no negative impact on the conversion of wollastonite under the chosen experimental conditions (Fig. 11a). Thus, this alternative cement system shows promise for a potential future use for well plugging warranting further investigations, e.g. of its long-term stability.

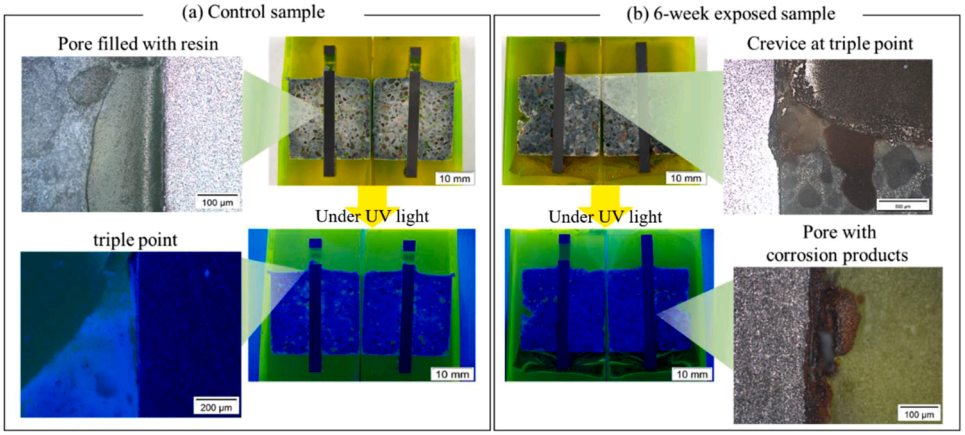

Fig. 9. Microscopic images at the interface of L485MB/Variodur coupons (a) reference, and (b) after six weeks of exposure in CO_2-saturated synthetic formation water at a pressure of 10 MPa and a temperature of 333 K. The coupons were embedded in fluorescencing epoxy resin, then cut and ground, cleaned and dried up before imaging. All preparation steps were carried out without using water to avoid corrosion.

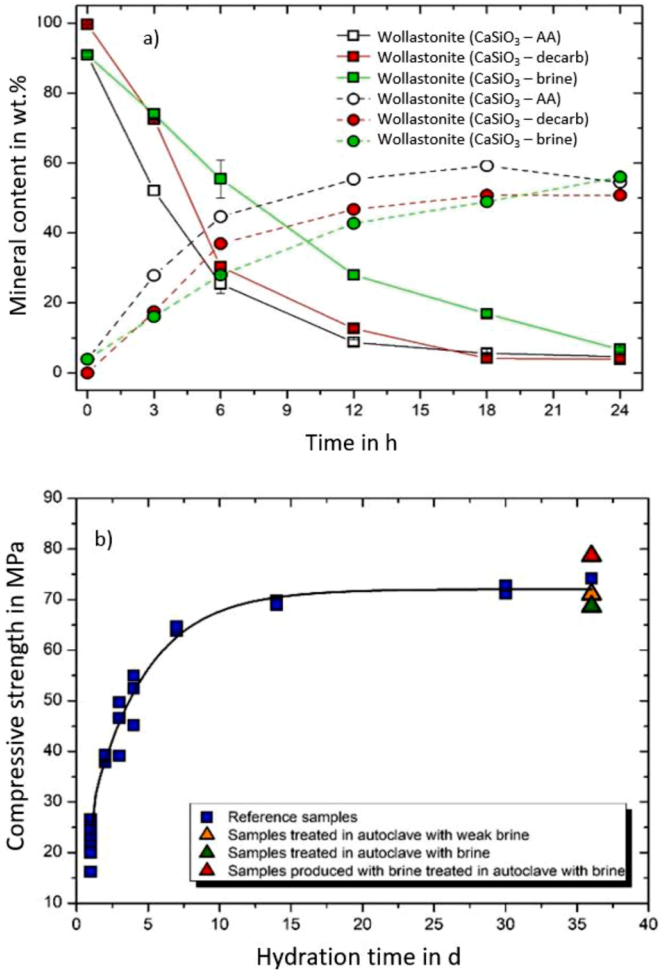

Fig. 11. a) Results of different wollastonite carbonation experiments (at a temperature of 333 K and a pressure of 2 MPa); $CaSiO_3$-AA: untreated wollastonite powder in H_2O/pure CO_2 (black line); $CaSiO_3$-decarb: wollastonite powder decarbonated by HCl treatment in H_2O/pure CO_2 (red line); $CaSiO_3$-brine: untreated wollastonite powder in brine/CO_2 (incl. SO_2 and $NO_2$70 ppm each; green line). Squares: wollastonite concentration; circles: carbonate concentration. Please note: Each data point corresponds to at least two measurements. In some cases, symbols used for data points are larger than corresponding error bars. b) Compressive strength of CEM III mortar prisms at different hydration time (according to DIN EN 196–1:2005) and varied conditions.

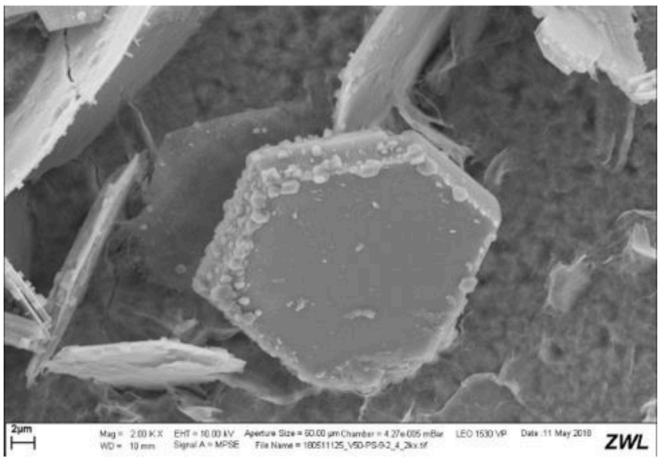

Fig. 12. SEM-image of pseudo-hexagonal hydrocalumite (AFm) inside the pores of the treated mortar prisms.

5. Impacts on geological CO_2 storage

5.1. Dissolution of SO_2

One main control on the extent of "gas"-fluid-rock reactions in saline aquifers is the partitioning behavior of impurities from the dense CO_2 phase into formation water. For SO_2 at a concentration of 440 ppm_v in a dense CO_2 phase, the partitioning was investigated in stirred 200 ml all-titanium high pressure reactors under assumed in situ reservoir conditions of 16 MPa pressure and 333 K temperature for three different scenarios: 1.) a dense CO_2 phase in contact with 125 ml pure H_2O, 2.) a dense CO_2 phase in contact with 125 ml brine (250 g/l NaCl), and 3.) a dense CO_2 phase in contact with 125 ml pure H_2O and O_2 (1,700 ppm) added (see also Fuhrmann et al., 2019). For the batch system with pure H_2O, 65% of the SO_2 initially present in the dense CO_2 phase partitioned into the H_2O, 35% of the SO_2 was remaining in the dense CO_2 phase. For the saline brine system, only 50% of the SO_2 partitioned into the brine after equilibration and more SO_2 remained in the dense CO_2 phase compared to the pure H_2O experiment. The solubility of SO_2 – and its dissociated sulfur species with an oxidation state of +IV – was 3.4 mmol/kgw for the pure H_2O system in comparison to 2.9 mmol/kgw for brine (see also Amshoff et al., 2018). If O_2 was present in the batch system, SO_2 completely partitioned into the aqueous phase (Fig. 13). Thus, redox conditions and brine salinities influence the amount of SO_2 dissolved in the formation water and the distance of SO_2 transport with the CO_2 plume in the storage reservoir (see also below).

The partitioning of SO_2 from the dense CO_2 phase into the aqueous fluid is not instantaneous (Fig. 13). The kinetics of the mass transfer of SO_2 into the aqueous fluids was investigated in a series of experiments with different hydrodynamic conditions (i.e. stirring intensities in the high-pressure reactors). The mass transfer coefficients K_L of SO_2 into pure H_2O were significantly higher (38.6 cm^{-1}/h) than those of CO_2 (15.8 cm^{-1}/h), corrobating the notion of the preferential partitioning of SO_2 from the migrating CO_2 plume into the formation water. An increased salinity (250 g/l NaCl) slowed down the mass transfer – for SO_2 to 24.0 cm^{-1}/h, for CO_2 to 11.8 cm^{-1}/h – again pointing to a potentially prolonged SO_2 transport with the migrating CO_2 plume in the storage reservoir despite the SO_2's high water solubility. These results imply that kinetic data on the mass transfer of impurities and the consecutive impurity reactions should be included in predictive models simulating reactive flow and the extent of geochemical reactions in the reservoir. Equilibrium approaches may significantly overestimate near-injection well reactions, on the one hand, and underestimate the transport of impurities into the reservoir, on the other.

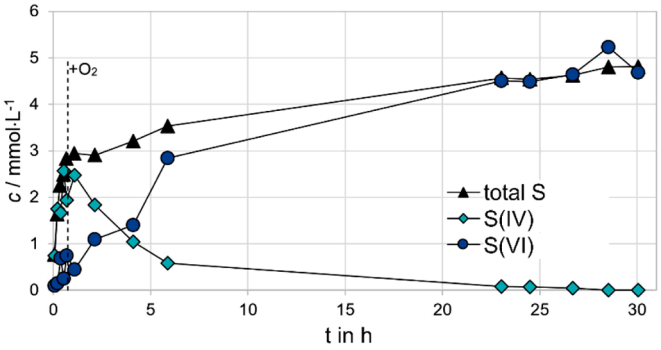

Fig. 13. Total sulfur concentration and concentrations of S (IV) and S (VI) species in brine in dissolution experiment with CO_2 containing SO_2 at a concentration of 440 ppm_v. In addition, O_2 was injected 40 min. after experiment start (indicated by dotted line) to reach a final CO_2 stream concentration of 1700 ppm_v. Most experiments were repeated at least once.

5.2. Fluid-mineral reactions – laboratory experiments

The geochemical conditions in the storage reservoir might be affected by impurities in the dense CO_2 stream leading to direct "gas"-(fluid-)mineral-reactions. For example, impurities may change the pH value of the formation water due to their dissolution. In addition, reactions of dissolved and dissociated impurity species in the formation water with other ions or mineral surfaces may occur. Reactions governed by redox processes were investigated in detail in this study, mainly involving SO_2 and molecular hydrogen (H_2). The results highlight the importance of spatially closely coupled redox-dissolution-re-precipitation processes during geological CO_2 storage. One example is the reduction of hematite (Fe_2O_3) surfaces, a mineral ubiquitous in sandstone reservoirs, by molecular H_2 and the subsequent formation of iron carbonates from CO_2 or its dissociated species in an aqueous fluid on the evolving mineral surface (Fig. 14). Unexpectedly, this reaction was also observed in experiments without H_2O being initially present. Apparently, the reduction of hematite by H_2 produces H_2O as an oxidation product of H_2. This H_2O appears to form small domains on the mineral surface, in which CO_2 can dissolve and then partake in the precipitation of iron carbonate. The extent and the geotechnical relevance of the production of small amounts of H_2O in an otherwise dry environment in storage reservoirs warrants further investigations. If future research shows that this process is of geotechnical relevance, it should be included, for example, in geochemical models of the dry-out zone in the vicinity of boreholes during injection of a H_2-bearing CO_2 phase. Complementary to the experiments described in Section 4.2, "geochemical" core flooding experiments with a dense CO_2 stream containing 50 ppm of SO_2 were performed using sandstone cores (Grauer Wesersandstein, size: 20 mm x 60 mm) under assumed reservoir conditions of 16 MPa fluid pressure and a temperature of 333 K. These experiments did not result in significant changes of the permeability of the rock cores as pressure differences over the rock core were the same in pure and impure CO_2 experiments. Corrobating these findings on the constant injectivity, imaging of the rock cores before and after the core flooding experiments by X-ray computer tomography (μCT) did not reveal any changes in porosity. Consequently, the impact of geochemical reactions on these physical rock parameters was negligible. This corresponds with the findings of, for example, Pearce et al. (2016) and of our geochemical simulations (see Section 5.3).

5.3. Reactive transport processes – modeling studies

In order to simulate the effects of temporally variable CO_2 stream compositions on reservoir rocks, an innovative modeling approach for TOUGHREACT V3.0-OMP was developed within the CLUSTER project (see also Wolf, 2017). In brief, this "hybrid approach" is based on i) the "gas" saturation profile for a pure CO_2 injection scenario and ii) an injection of pre-calculated amounts of each dissolved impurity into specific grid cells of the reservoir model at certain time steps. Hence, CO_2-phase transport and dissolution of impurities is mimicked by "moving the point of injection" through the individual grid cells of the reservoir model (see also Wolf et al., 2017). For studying the impact of geochemical reactions in two generic sandstones from the Buntsandstein – the Grauer Wesersandstein and one with an "average composition" of Buntsandstein sandstones in the North German Basin (Waldmann et al., 2014) – a set of multiphase reactive transport simulations was performed. Simulations comprised the injection of CO_2 containing temporally varying concentrations of SO_2, NO_2, O_2 and H_2 into a 1D radial symmetric reservoir at a pressure of 16 MPa and a temperature of 333 K. Average impurity concentrations were 17 ppm SO_2, 42 ppm NO_2, 2040 ppm O_2 and 1061 ppm H_2 based on the calculated variation at the end of the trunk line in the CCS cluster scenario (see also Section 2). Model input parameters, impurity concentrations and impurity combinations were varied during the set of reactive transport simulations. This was done to evaluate the sensibilities of different input parameters and impurities, on the one hand, and to be able to estimate their influence on porosity and permeability of the reservoir rock, on the other.

Modeling results show that simulated mineralogical changes strongly depend on the impurities present and on the primary mineral phases of the scenario. Main geochemical-mineralogical reactions occur with Ca- and Fe-bearing phases. On the one hand, acidifying impurities trigger acid-induced reactions of Ca-rich minerals, namely dissolution of carbonates and precipitation of anhydrite. On the other hand, redox-sensitive impurities control redox reactions with Fe-rich minerals, namely dissolution of chlorite and precipitation of goethite (Fig. 15).

In summary, the set of simulations for the two sandstones from the Buntsandstein shows that mineral reactions during the storage of CO_2-SO_2-NO_2-O_2-H_2 mixtures are limited: the modelled impacts of impurities on the porosity of the investigated sandstones were negligible and within the natural variability of the considered sandstones in the CCS cluster scenario. Similar modeling results have been obtained by, for example, Pearce et al. (2015 & 2019) who studied geochemical impacts of CO_2-SO_2 and CO_2-SO_2-O_2 mixtures, respectively, in siliciclastic sandstones.

5.4. Rock alteration and geomechanical implications

Batch alteration experiments with CO_2 containing SO_2 and NO_2 (70 ppm_v each; in highly saline brine at a pressure of 16 MPa and a temperature of 333 K for five weeks) and subsequent geomechanical tests

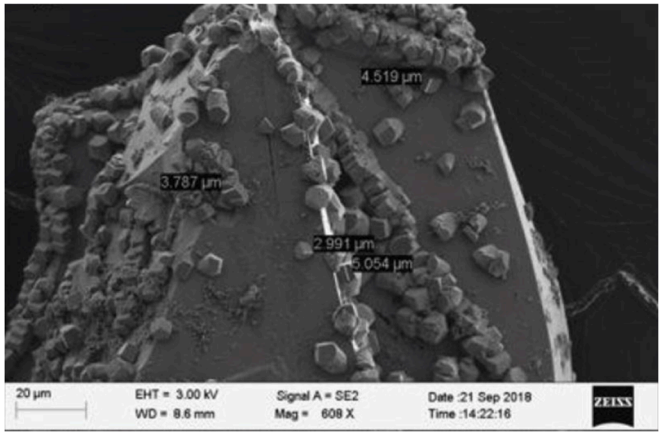

Fig. 14. Surface of an iron oxide (hematite) grain with small crystals of newly precipitated iron carbonate (siderite) formed during the reaction with dense CO_2 and H_2 (CO_2:H_2 ratio is 89:3) at simulated in situ conditions.

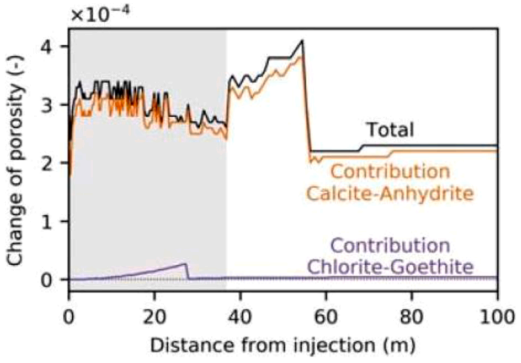

Fig. 15. Simulated changes of total porosity including individual contributions of the coupled mineral reactions after one year of injection exemplarily shown for a scenario using an "averaged" sandstone composition of Buntsandstein from the North German Basin and a CO_2 stream containing SO_2, NO_2, O_2 and H_2 in temporally varying concentrations.

were carried out with rock cores (14 cm length, 7 cm diameter) of the Grauer Wesersandstein. An in-depth description of the geomechanical/-chemical and mineralogical investigation is given in Neumann et al. (2018), Menezes (2019), Menezes and Lempp (2018) and Menezes et al. (2018). Visual inspection and μCT analysis showed that the investigated sandstone contains low-density domains of different sizes and shapes. By comparing selected regions of mineral surfaces by digital microscopy before and after the alteration experiments, no clear evidence for alterations due to the treatment with brine (250 g/l) saturated with impure CO_2 was found. SEM analyses supported these results.

As examples of the results of the geomechanical studies, Figs. 16a-d show the pore fluid volume changes of untreated rock cores, i.e. the fluid volume necessary to maintain constant pressure during a triaxial experiment with a duration of several hours. It is apparent that the fluid volumes vary widely and depend on the presence of low-density domains in the rock: If these are absent (Fig. 16a, green line), the pore fluid volume change is nearly independent of axial deformation. In addition, these rock cores showed a higher than average dry density, a reduced effective porosity and higher compressive strength (details are given in Menezes et al., 2018).

Fig. 16b-d show the pore fluid volume change as a function of axial volume change during triaxial loading: A dependence of the pore fluid volume change on the direction of axial deformation was observed (see also Menezes (2019), Menezes and Lempp (2018), Menezes et al. (2018), Neumann et al. (2018)). For cores drilled perpendicular to the bedding, the difference between data for cores altered in brine and N_2 or CO_2-impurity mixtures (Fig. 16b) was more pronounced than for cores drilled parallel to the bedding (here: comparison of untreated cores and cores treated with brine/impure CO_2, Fig. 16c,d). The pore fluid volume change was significantly larger for the core treated with N_2/brine. This core also showed mechanical failure at larger axial volume changes in comparison to the core treated with impure CO_2 (see red star symbols). However, the shear stress τ of the latter was higher than that of the sample exposed to N_2. Cores that were drilled parallel to the bedding overall displayed a smaller pore fluid volume change in comparison to the perpendicularly drilled cores. Mechanical failure was observed at similar axial deformation and volume change for all cores irrespective of samples treatment. However, the shear stress τ (Fig. 16c) was higher for the core exposed to CO_2 and impurities in comparison to the untreated sample (cf. Fig. 16d).

Overall, the observed differences of the geomechanical properties between individual rock samples – irrespective of treatment – mainly reflect the inherent natural variability of the investigated rock samples of Grauer Wesersandstein. The natural variability of geomechanical rock properties in the Grauer Wesersandstein was found to be higher than any alterations observed after 5-week batch experiments with impure CO_2. This finding points to a potentially good suitability of such silicate-cemented rocks for storage of impure CO_2 streams.

6. Recommendations

Based on all project results, the project team recommends defining minimum composition thresholds for CO_2 streams not as strict threshold values for each individual impurity in a CO_2 stream, but rather by constraining the CO_2 stream composition and its variability for a specific CCS project with regard to the following parameters:

i) overall CO_2 purity; maximum contents of relevant impurities and/or
ii) maximum total element contents;
iii) acceptable variabilities of impurity contents;
iv) impurity combinations to be avoided.

No substantial technical obstacles for transporting, injecting and storing CO_2 streams with temporally variable compositions and mass flow rates as considered in our CCS cluster scenario were found. Thus, the considered CO_2 stream compositions and their variabilities (cf. Table 1) can be taken as acceptable for CO_2 pipeline transport, injection and storage. For illustration, the parameters listed above are exemplarily detailed in Table 2 for the considered CCS cluster scenario.

It should be pointed out that our results were derived for a partially simplified model CCS cluster system. For example, for the pipeline

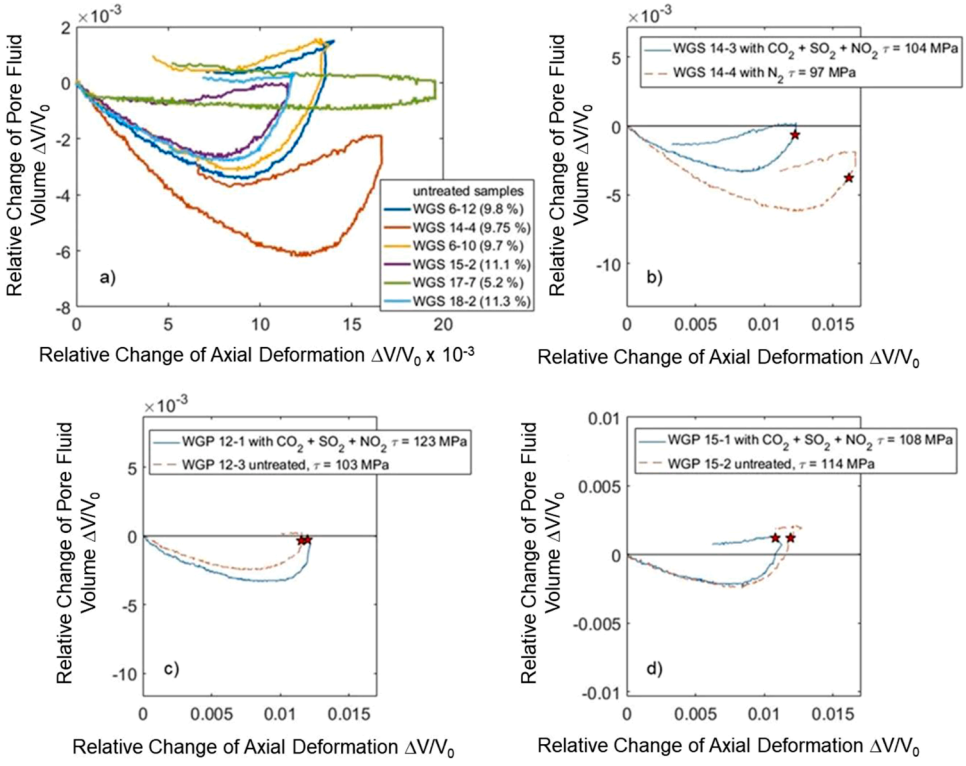

Fig. 16. Pore fluid volume changes of different sandstone cores as a function of the axial deformation in triaxial tests (different colours indicate individual samples; figures modified after Menezes, 2019) and dependence of the pore fluid volume change on the core drilling direction and the sample treatment – a) untreated samples (cores drilled perpendicular to bedding; measured effective porosities are given in the legend); b) samples treated in brine with N_2 (orange line) or with CO_2 containing NO_2 and SO_2 (70 ppm_v each; blue line) (core drilled perpendicular to the bedding). c) and d) untreated samples (orange line) and samples loaded with CO_2 containing NO_2 and SO_2 (70 ppm_v each; blue line) (cores drilled parallel to bedding). Red star symbols indicate the point of the maximum shear stress of the sample before mechanical failure.

Table 2
Detailing of recommended parameters for CCS cluster scenario.

Parameter	Exemplary details according to CCS cluster scenario	Comment
Overall CO_2 purity	$\geq$ 98.6 mol% CO_2 for transport, 98.9 mol% for injection and storage	No constraints found for theses purities during transport, injection and storage
Maximum contents of relevant impurities	H_2O content: $\leq$ 50 ppm_v	H_2O content identified as relevant for acid formation and corrosion
	SO_3 proportion in SO_x: 1:3.5	SO_3 rapidly forms H_2SO_4 with available H_2O, whereas SO_2 needs further redox active impurities for fast conversion
Maximum total element contents	Total S content (cf. Table 1)	Due to oxidation of reduced S-containing impurities at mixing with oxidizing CO_2 streams and consecutive acid formation, see also below
Acceptable variabilities of impurity contents	Variation between 0 and maximum concentration indicated in Table 1	Some effects of varying CO_2 stream compositions detected, but no severe constraints found for impurities and variabilities considered
Impurity combinations to be avoided	Mixing of CO_2 streams containing impurities with oxidizing properties and streams with S-bearing impurities	Limit oxidation and acid formation reactions in CO_2 streams; see above

transport studies, a straight-line pipeline with constant elevation was assumed and no variations in soil properties such as temperature were considered. In addition, impacts of impurities with oxidizing properties and/or from which acids may be formed were studied in more detail in the CLUSTER project, while fewer investigations addressed impacts of impurities with reducing properties. Thus, our database for recommendations derived from impacts of the latter is smaller and results are associated with larger uncertainties. To fully optimize CO_2 stream compositions and specify these recommended parameters in more detail, further studies are needed involving, for example, higher impurity concentrations, a broader range of impurities with reducing properties and more realistic settings and scales.

The optimization of CO_2 stream composition may be particularly challenging for those impurities that have negative impacts in one part of the CCS system, but may be beneficial in other parts. Such an example is H_2 that, e.g., challenges the economics of CO_2 ship transport (see also Engel and Kather, 2018), but can promote CO_2 mineral trapping by carbonate formation in the presence of Fe(III)-bearing minerals in the storage reservoir (see Section 5.2). For these impurities, the defintion of acceptable concentration thresholds may involve balancing benefits and trade-offs if the latter cannot be mitigated otherwise.

The available ISO standards for pipeline transportation (ISO 27913:2016) and geological storage (ISO 27914:2017) provide no strict guidance for specifying CO_2 stream compositions, only "indicative levels of main CO_2 impurities and factors driving these levels" are listed in the annex of ISO 27913:2016. The proposed CO_2 specifications for the Northern Lights and the Goldeneye projects set very high purity requirements, whereas other published CO_2 qualities for design studies consider lower CO_2 purities (e.g., Dugstad and Svennigsen, 2019, and references therein). For example, proposed maximum H_2O contents are 30 and 50 ppm_v for the Northern Lights and Goldeneye projects, respectively, which are similar to the H_2O content used and found to be acceptable in our studies. Overall, the CO_2 specification for the Goldeneye and Northern Lights projects rigorously limit contents of all potentially reactive impurities such as O_2, NO_x and SO_x, but also of H_2S and H_2 to much lower values than those considered in the CLUSTER project. It is important to note that CO_2 stream compositions to be used in real CCS projects are controlled by a variety of project-specific settings and constraints all along the CCS chain – from CO_2 sources to the storage reservoir (e.g., Dugstad and Svennigsen, 2019). Hence, site- and project-specific studies are mandatory.

7. Conclusions

As mentioned above, no substantial technical obstacles were detected for transporting, injecting and storing CO_2 streams with temporally variable compositions and mass flow rates as studied in the project's CCS cluster scenario. Materials suitable for handling these variable streams were identified including steels for pipelines and injection tubing as well as cement systems for well cementation or plugging. Due to their low geochemical reactivity, silicate-cemented sandstones can be particularly suitable for storing impure CO_2 streams with a variable composition. In the CLUSTER project, most pronounced impurity effects were found in the pipeline corrosion studies and related modeling of cross-chemical reactions in CO_2 streams. Thus, the parameters recommended for constraining CO_2 stream composition are primarily based on these results pointing to the importance of cross-chemical reactions, acid formation and corrosion during pipeline transport in the project's CCS cluster scenario. For limiting cross-chemical reactions in CO_2 streams, variations of redox conditions in the CO_2 stream and at CO_2 stream mixing points, e.g., at pipeline network junctions, are of particular importance. However, real CCS projects may have other constraining factors limiting CO_2 stream composition and acceptable variations thereof.

Note that an interactive webtool providing an overview presentation of key results from the CLUSTER project is available on the project homepage at www.bgr.bund.de/CLUSTER.

CRediT authorship contribution statement

Heike Rütters: Conceptualization, Writing – review & editing, Supervision, Writing – original draft, Project administration, Formal analysis, Funding acquisition. **Sebastian Fischer:** Conceptualization, Writing – review & editing, Writing – original draft, Supervision, Resources, Project administration, Formal analysis. **Le Quynh Hoa:** Data curation, Writing – original draft, Visualization, Investigation. **Dirk Bettge:** Funding acquisition, Validation, Supervision, Resources, Project administration, Methodology. **Ralph Bäßler:** Funding acquisition, Supervision. **Jobst Maßmann:** Funding acquisition, Writing – original draft, Validation, Supervision, Methodology. **Christian Ostertag-Henning:** Data curation, Writing – original draft, Visualization, Validation, Supervision, Investigation, Funding acquisition. **J. Lennard Wolf:** Data curation, Validation, Software, Methodology, Investigation. **Martin Pumpa:** Data curation, Writing – original draft, Visualization, Software, Methodology, Investigation. **Udo Lubenau:** Data curation, Writing – original draft, Visualization, Software, Resources, Project administration, Methodology, Investigation. **Sandra Knauer:** Data curation, Writing – original draft, Visualization, Supervision, Validation, Methodology, Investigation. **Philip Jaeger:** Data curation, Resources, Project administration, Investigation. **Andreas Neumann:** Data curation, Writing – original draft, Visualization, Validation, Investigation. **Kristoff Svensson:** Data curation, Writing – original draft, Validation, Investigation. **Herbert Pöllmann:** Funding acquisition, Validation, Supervision, Resources, Project administration, Methodology. **Christof Lempp:** Funding acquisition, Validation, Methodology, Supervision. **Flora F. Menezes:** Data curation, Validation, Investigation. **Birger Hagemann:** Data curation, Writing – original draft, Resources, Validation, Project administration, Investigation.

Declaration of Competing Interest

The authors declare that they have no known competing financial

interests or personal relationships that could have appeared to influence the work reported in this paper.

Acknowledgements

The project CLUSTER was funded by the German Federal Ministry of Economic Affairs and Energy (BMWi) on the basis of a decision by the German Bundestag (Grant No. 03ET7031A to G). The authors acknowledge the fruitful collaboration with the Institute for Energy Technologies, Hamburg University of Technology. We also would like to thank the two anonymous reviewers for their constructive comments that helped to substantially improve the manuscript.

References

Amshoff, P., Weger, T., Ostertag-Henning, C., 2018. Dissolution kinetics of CO_2 and CO_2-SO_2 mixtures in water and brine at geological storage conditions of 16MPa and 333K. Int. J. Greenh Gas Con. 79, 173–180.

American Petroleum Institute—API, 1991. Recommended Practice for Design and Installation of Offshore Production Platform Piping Systems (API RP 14E). American Petroleum Institute, Washington, DC, USA.

Atkinson, R., Baulch, D.L., Cox, R.A., Crowley, J.N., Hampson, R.F., Hynes, R.G., Jenkin, M.E., Rossi, M.J., Troe, J., 2004. Evaluated kinetic and photochemical data for atmospheric chemistry: volume I - gas phase reactions of O_x, HO_x, NO_x and SO_x species. Atmos. Chem. Phys. 4, 1461–1738.

Bachu, S., Bennion, D.B., 2009. Experimental assessment of brine and/or CO_2 leakage through well cement at reservoir conditions. Int. J. Greenh Gas Con. 3, 494–501.

Baulch, D.L., Cobos, C.J., Cox, R.A., Esser, C., Frank, P., Just, T., Kerr, J.A., Pilling, M.J., Troe, J., Walker, R.W., Warnatz, J., 1992. Evaluated kinetic data for combustion modelling. J. Phys. Chem. Ref. Data 21, 411–429.

Brunsvold, A., Jakobsen, J.P., Mazzetti, M.J., Skaugen, G., Hammer, M., Eickhoff, C., Neele, F., 2016. Key findings and recommendations from the IMPACTS project. Int J Greenh Gas Con 54, 588–598.

Choi, Y.-S., Nesic, S., Young, D., 2010. Effect of impurities on the corrosion behavior of CO_2 transmission pipeline steel in supercritical CO_2-water environments. Environ. Sci. Technol. 44, 9233–9238.

DIN EN 196-1:2005, 2005. Methods of testing cement – Part 1: determination of strength, German version EN 196-1_2005. Deutsches Institut für Normung e.V. Beuth Verlag.

DIN EN 10208-2:2009, 2009. Steel pipes for pipelines for combustible fluids - Technical delivery conditions - Part 2: pipes of requirement class B; German version EN 10208-2:2009. Deutsches Institut für Normung e.V. Beuth Verlag.

Dugstad, A., Svennigsen, G., 2019. Variation in CO_2 composition – defining safe operation windows. Recommendations on CO_2 specification for ALIGN partners. ALIGN CCUS Deliverable No. D2.3.3 19.

Engel, F., Kather, A., 2018. Improvements on the liquefaction of a pipeline CO_2 stream for ship transport. Int. J. Greenh. Gas Con 72, 214–221.

Fuhrmann, L., Amshoff, P., Grunwald, N., Fischer, S., Maßmann, J., Ostertag-Henning, C., Wolf, L., Rütters, H., 2019. CLUSTER – Projektteil der BGR: potenzielle Auswirkungen von zeitlich variierenden CO_2-Strömen auf injektionsrelevante Prozesse im Speicher und Prognosen zu möglichen Verformungen der Geländeoberfläche. Final Report Bundesanstalt für Geowissenschaften und Rohstoffe: Berlin/Hannover;.

Gassnova, S.F., 2020. Developing Longship – key lessons learned. Report 47.

Grunwald, N., Maßmann, J., Kolditz, O., Nagel, T., 2020. Non-iterative phase-equilibrium model of the H_2O-CO_2-NaCl-system for large-scale numerical simulations. Math. Comput. Simul 178, 46–61.

Hagemann, B., Strobel, G., Kroll, J., Ganzer, L., 2018. Core flooding experiments related to the injectivity during CO_2 storage with impurities under in-situ conditions. In: 14th Greenhouse Gas Control Technologies Conference Melbourne 21-26 October 2018 (GHGT-14). Available at SSRN. https://ssrn.com/abstract=3365972.

Hua, Y., Barker, R., Neville, A., 15-19 April 2018. Corrosion behaviour of X65 steels in water-containing supercritical CO_2 environments with NO_2/O_2. In: Proceedings of the CORROSION 2018. NACE International, Phoenix, AZ, USA, p. 11085.

Hunter, I., 2021. CCS infrastructure in the UK. – Webinar slides; GCCSI Webinar. CCS infrastructure in the UK. Available at. https://www.globalccsinstitute.com/resources/multimedia-library/the-carbon-capture-and-storage-101-webinars-ccs-infrastructure-for-a-net-zero-future/.

IEA, G.H.G., 2015. Carbon capture and storage cluster projects: review and future opportunities. Report 139, 2015/03.

ISO 27913, 2016. Carbon dioxide capture, transportation and geological storage - pipeline transportation systems. ISO/TC 265, 35.

ISO 27914, 2017. Carbon dioxide capture, transportation and geological storage - geological storage. ISO/TC 265, 59.

ISO/TR 27921, 2020. Carbon dioxide capture, transportation and geological storage – cross cutting issues – CO_2 stream composition. ISO/TC 265, 45.

Kahlke, S.-L., Pumpa, M., Schütz, S., Kather, A., Rütters, H., 2020. Potential dynamics of CO_2 stream composition and mass flow rates in CCS clusters. Processes 8, 1188.

Kather, A., Kahlke, S.-L., Engel, F., 2019. Cluster – Endbericht des Teilprojekts: Definition der CO_2-Quellen, Quellenbilanzierung, Interaktion Quelle/Transportnetz, Schiffstransport. Final Report Institut für Energietechnik der Technischen Universität Hamburg, Hamburg, Germany.

Kaufmann, D., Heim, S., Jähne-Klingberg, F., Steuer, S., Bebiolka, A., Wolf, M., Kuhlmann, G., 2014. GSN – Generalisiertes, Erweitertes Strukturmodell des Zentralen Deutschen Nordsee-Sektors – Konzept Zur Erstellung einer Konsistenten Datengrundlage für weiterführende Modellierungen im Bereich des Zentralen Deutschen Nordsee-Sektors. Bundesanstalt für Geowissenschaften und Rohstoffe: Hannover, Germany. Report.

Kelly, R.G., Lee, J.S., 2018. Localized corrosion: crevice corrosion. Encycl. Interfac. Chem. 291–301.

Knauer, S., Le, Q.H., Baessler, R., Jaeger, P., 2019. Contact angle and corrosion of a water-CO_2 system on X70 and S41500 at 278 K and pressures up to 20MPa. Int. J. Greenh. Gas Con. 89, 33–39.

Kolditz, O., Bauer, S., Bilke, L., Böttcher, N., Delfs, J.O., Fischer, T., Görke, U.J., Kalbacher, T., Kosakowski, G., McDermott, C.I., Park, C.H., Radu, F., Rink, K., Shao, H., Shao, H.B., Sun, F., Sun, Y.Y., Singh, A.K., Taron, J., Walther, M., Wang, W., Watanabe, N., Wu, N., Xie, M., Xu, W., Zehner, B., 2012. OpenGeoSys: an open-source initiative for numerical simulation of thermo-hydro-mechanical/chemical (THM/C) processes in porous media. Environ. Earth Sci. 67, 589–599.

Kratzig, A., Bettge, D., Le, Q.H., Bäßler, R., Kranzmann, A., 2018. Interaction of oxidizing and reductive components in CO_2 streams with transport pipeline steel X70 at high pressure and low temperature. In: 14th Greenhouse Gas Control Technologies Conference Proceeding, Melbourne 21-26 October (GHGT-14).

Kratzig, A., Le, Q.H., Bettge, D., Menneken, M., Bäßler, R., 2020. Early Stage of Corrosion Formation on Pipeline Steel X70 Under Oxyfuel Atmosphere at Low Temperature. Processes 8, 421.

Kumar, G., Prabhu, K.N., 2007. Review of non-reactive and reactive wetting of liquids on surfaces. Adv. Colloid Interface Sci. 61–89.

Kunz, O., Wagner, W., 2012. The GERG-2008 wide-range equation of state for natural gases and other mixtures: an expansion of GERG-2004. J. Chem. Eng. Data 57, 3032–3091.

Le, Q.H., Bäßler, R., Knauer, S., Jaeger, P., Bettge, D., Kratzig, A., Kranzmann, A., 2018. Droplet corrosion of CO_2 transport pipeline steels in simulated oxyfuel flue gas. Corrosion 74, 1406–1420.

Le, Q.H., Bäßler, R., Bettge, D., Buggisch, E., Schiller, B.N., Beck, M., 2021. Corrosion study on wellbore materials for the CO_2 injection process. Processes 9 (1), 115.

Lemmon, E.W., Huber, M.L., McLinden, M.O., 2013. REFPROP: reference fluid thermodynamic and transport properties. NIST Standard Ref. Database 23.

Lubenau, U., Pumpa, M., Schütz, S., Barsch, M., 2019. CLUSTER-Einfluss Von CO_2-Begleitkomponenten auf die Auslegung und Gestaltung des Transportnetzes und Der Obertageanlage. Final Report DBI Gas- und Umwelttechnik GmbH, Leipzig, Germany.

Menezes, F.F., 2019. Anisotropy of volume change and permeability evolution of hard sandstones under triaxial stress conditions. J. Petrol. Sci. Eng. 174, 921–939.

Menezes, F.F., Lempp, C., 2018. On the structural anisotropy of physical and mechanical properties of a Bunter Sandstone. J. Struct. Geol. 114, 196–205.

Menezes, F.F., Lempp, C., Svensson, K., Neumann, A., Pöllmann, H., 2018. Geomechanical behaviour changes of a Bunter Sandstone and of a borehole cement due to CO_2 injection effects. In: Proc JAEG/AEG Annual Meeting San Francisco, 1, pp. 111–118.

Morland, B.H., Norby, T., Tjelta, M., Svenningsen, G., 2019a. Effect of SO_2, O_2, NO_2, and H_2O concentrations on chemical reactions and corrosion of carbon steel in dense phase CO_2. Corrosion 75 (11), 1327–1338.

Morland, B.H., Tjelta, M., Norby, T., Svenningsen, G., 2019b. Acid reactions in hub systems consisting of separate non-reactive CO_2 transport lines. Int. J. Greenh. Gas Control 87, 246–255.

Morland, B.H., Tadesse, A., Svenningsen, G., Springer, R.D., Anderko, A., 2019c. Nitric and sulfuric acid solubility in dense phase CO_2. Ind. Eng. Chem. Res. 58, 22924–22933.

Munkjord, S.T., Hammer, M., Lovseth, S.W, 2016. CO_2 transport: data and models - a review. Appl. Energy 169, 499–523.

Neele, F., Gittins, C., Wildenborg, T., Mikunda, T., 2018. Initiating large-scale storage in the Netherlands offshore. In: 14th Greenhouse Gas Control Technologies Conference Melbourne 21-26 October. https://doi.org/10.2139/ssrn.3366065 (GHGT-14).

Neumann, A., Svensson, K., Pöllmann, H., Menezes, F.F., Lempp, C., 2018. Mineralogical analyses of the impact of CO2 and associated compounds on sandstone in the presence of formation waters at non ambient conditions. In: 40th ICMA Conference. Miami.

Pearce, J.K., Golab, A., Dawson, G.K., Knuefing, L., Goodwin, C., Golding, S.D., 2016. Mineralogical controls on porosity and water chemistry during O_2-SO_2-CO_2 reaction of CO_2 storage reservoir and cap-rock core. Appl. Geochem. 75, 152–168.

Pearce, J.K., Kirste, D.M., Dawson, G.K., Farquhar, S.M., Biddle, D., Golding, S.D., Rudolph, V., 2015. SO_2 impurity impacts on experimental and simulated CO_2–water–reservoir rock reactions at carbon storage conditions. Chem. Geol. 399, 65–86.

Pearce, J.K., Kirste, D.M., Dawson, G.K.W., Rudolph, V., Golding, S.D., 2019. Geochemical modelling of experimental O_2–SO_2–CO_2 reactions of reservoir, cap-rock, and overlying cores. Appl. Geochem. 109, 104400.

Peletiri, S.P., Rahmanian, N., Mujtaba, I.M., 2017. Effects of impurities on CO_2 pipeline performance. Chem Eng Trans 57, 6.

Peletiri, S.P., Mujtaba, I.M., Rahmanian, N., 2019. Process simulation of impurity impacts on CO_2 fluids flowing in pipelines. J Clean P 240, 118145.

Peletiri, S.P., Rahmanian, N., Mujtaba, I.M., 2018. CO2 pipeline design: a review. Energies 11 (9), 2184.

Porter, R.T.J., Mahgerefteh, H., Brown, S., Martynov, S., Collard, A., Woolley, R.B., Fairweather, M., et al., 2016. Techno-economic assessment of CO_2 quality effect on its storage and transport: CO2QUEST: An overview of aims, objectives and main findings. Int. J. Greenh. Gas Con. 54, 662–681.

Ratnayaka, D.D., Brandt, M.J., Johnson, K.M., 2009. Pipeline design and construction. Chapter 15, Water Supp. (Sixth Ed.) 561–598.

Rütters H., Abbasi N., Amshoff P., Barsch M., Bäßler R., Bettge D., Engel F., Fischer S., Fuhrmann L., Grunwald N., Hagemann B., Jaeger P., Kahlke S.-.L., Kleinickel C., Knauer S., Le Q.-.H., Lempp C., Lubenau U., Maßmann J., Menezes F.F., Neumann A., Ostertag-Henning C., Pöllmann H., Pumpa M., Schulz S., Strobel G., Svensson K., Wolf J.L. CLUSTER – Abschlusssynthese. – Report, Bundesanstalt für Geowissenschaften und Rohstoffe: Hannover, Germany; 2019.

Rütters, H., Stadler, S., Bäßler, R., Bettge, D., Jeschke, S., Kather, A., Lempp, C., Lubenau, U., Ostertag-Henning, C., Schmitz, S., Schütz, S., Waldmann, S., 2016. Towards an optimization of the CO_2 stream composition - a whole-chain approach. Int. J. Greenh. Gas Con. 54, 682–701.

Spitz, T., Avagyan, V., Ascui, F., Bruce, A.R.W., Chalmers, H., Lucquiaud, M., 2018. On the variability of CO_2 feed flows into CCS transportation and storage. Int. J. Greenh. Gas Control. 74, 296–311.

Stewart, M., 2016. Material requirements: piping materials. Chapter 3, Surf. Prod. Oper. 159–192.

Svensson, K., Neumann, A., Menezes, F.F., Lempp, C., Pöllmann, H., 2018. The conversion of wollastonite to $CaCO_3$ considering its use for CCS application as cementitious material. Appl. Sci. 8, 304.

Svensson, K., Neumann, A., Menezes, F.F., Lempp, C., Pöllmann, H., 2019a. Carbonation of natural wollastonite at non-ambient conditions relevant for CCS—the possible use as cementitious material in wellbores. Appl. Sci. 9, 1259.

Svensson, K., Neumann, A., Menezes, F.F., Lempp, C., Pöllmann, H., 2019b. Carbonation of natural pure and impure wollastonite. Appl Sci 1, 318.

Svensson, K., Neumann, A., Menezes, F.F., Lempp, C., Pöllmann, H., 2020. Carbonation of CEM III mortar – influence of impure CO_2 (with SO_2 and NO_2) and chloride rich brine. Constr. Build. Mater. 260, 119831.

Weber, J., Ricken, W., 2005. Quartz cementation and related sedimentary architecture of the Triassic Solling Formation, Reinhardswald Basin, Germany. Sediment. Geol. 175, 459–477.

Wolf, M., Steuer, S., Röhling, H.G., 2015. Jähne-Klingberg F. Lithofacies distribution in the Central European Basin: a 3D model of the Buntsandstein facies in the central German North Sea. Z Deutsch Ges Geowiss (ZDGG) 166, 341–359.

Waldmann S., Stadler S., Nowak T., Gröger-Trampe J., Heeschen K., Riße A., Ostertag-Henning C., Rütters H. Geochemische Reaktionen von CO2-Gasgemischen mit Speichergesteinen und Deckschichten – COORAL Final Report Bundesanstalt für Geowissenschaften und Rohstoffe: Hannover, Germany; 2014.

Wheler, J., Eddy, B., Pearson, J., Haunholter, A., 2020. The alberta carbon trunk line: alberta's newest carbon solution. – Webinar slides. GCCSI CCS Talks available at. https://www.globalccsinstitute.com/resources/multimedia-library/ccs-talks-the-alberta-carbon-trunk-line-albertas-newest-carbon-solution/.

Wolf, J.L., 2017. Methods for modelling and simulation of CO_2 impurities and their reactive transport in geological storage reservoirs. In: Wittmann, J. (Ed.), Simulation in Umwelt- und Geowissenschaften, Workshop Berlin 2017. Shaker Verlag.

Wolf, J.L., Fischer, S., Rütters, H., Rebscher, D., 2017. Reactive transport simulations of impure CO_2 injection into saline aquifers using different modelling approaches provided by TOUGHREACT V3.0-OMP. Procedia Earth Planet Sci 17, 480–483.

Young, T., 1805. An essay on the cohesion of fluids. Philos. Trans. R. Soc. London 65–87.

ZEP, 2011. European technology platform for zero emission fossil fuel power plants. The Costs of CO_2 storage, Report 42.